SCIENTIFIC REPORTS
nature research

Check for updates

OPEN

Optimization of spin Hall magnetoresistance in heavy-metal/ferromagnetic-metal bilayers

Łukasz Karwacki[1,2]✉, Krzysztof Grochot[2,3]✉, Stanisław Łazarski[2], Witold Skowroński[2], Jarosław Kanak[2], Wiesław Powroźnik[2], Józef Barnaś[1,4], Feliks Stobiecki[1] & Tomasz Stobiecki[2,3]

We present experimental data and their theoretical description on spin Hall magnetoresistance (SMR) in bilayers consisting of a heavy metal (H) coupled to in-plane magnetized ferromagnetic metal (F), and determine contributions to the magnetoresistance due to SMR and anisotropic magnetoresistance (AMR) in five different bilayer systems: W/$Co_{20}Fe_{60}B_{20}$, $Co_{20}Fe_{60}B_{20}$/Pt, Au/$Co_{20}Fe_{60}B_{20}$, W/Co, and Co/Pt. The devices used for experiments have different interfacial properties due to either amorphous or crystalline structures of constitutent layers. To determine magnetoresistance contributions and to allow for optimization, the AMR is explicitly included in the diffusion transport equations in the ferromagnets. The results allow determination of different contributions to the magnetoresistance, which can play an important role in optimizing prospective magnetic stray field sensors. They also may be useful in the determination of spin transport properties of metallic magnetic heterostructures in other experiments based on magnetoresistance measurements.

Spin Hall magnetoresistance (SMR) is a phenomenon that consists in resistance dependence on the relative orientation of magnetization and spin accumulation at the interface of ferromagnet and strong spin-orbit material (such as 5*d* metals[1–8], topological insulators[9], or some 2D systems [10]). In transition metals such as W and Pt, the spin accumulation results from spin current driven by the spin Hall effect (SHE)[11–14]. The spin current diffuses then into the ferromagnet or exerts a torque on the magnetization while being backscattered. Due to the inverse spin Hall effect (ISHE), the backscattered spin current is converted into a charge current that flows parallel to the bare charge current driven by external electric field, which effectively reduces the resistance[3,4]. One of the most important advantages of driving spin currents by SHE is that the spin currents can be induced by a charge current flowing in the plane of the sample[15]. This may remedy some obstacles on the road to further miniaturization of prospective electronic components, which have been encountered in spin-valves and magnetic tunnel junctions when the electric field is applied perpendicularly to interfaces. One of the drawbacks, however, is that the strength and effectiveness of such subtle effects depend strongly on the quality and spin properties of interfaces[16–23].

Although early SMR experiments were performed on heavy-metal/ferromagnetic-insulator bilayers[1], recent efforts are focused on the bilayers with ferromagnetic metallic layers, such as Co or $Co_{20}Fe_{60}B_{20}$ ones[5,7], which are currently more relevant for applications. When the magnetization is parallel to the spin accumulation, the spin current from the heavy-metal can easily diffuse into the ferromagnetic metal (influencing its spin transport properties and spin accumulation on the ferromagnetic metal side)[5,24–30]. This is especially important when an additional spin sink (another heavy-metal layer or an antiferromagnet) is on the other side of the ferromagnetic layer, where effects such as spin current interference might take place[6].

Moreover, as charge current flows in plane of the sample, additional phenomena may occur, such as anisotropic magnetoresistance (AMR) or anomalous Hall effect (AHE)[31–36]. These effects can obscure determination of spin transport parameters and make evaluation of the SMR contribution to the measured magnetoresistance more difficult. Since the determination of such transport properties as the spin Hall angle (which parameterizes

[1]Institute of Molecular Physics, Polish Academy of Sciences, ul. M. Smoluchowskiego 17, 60-179 Poznań, Poland. [2]Department of Electronics, AGH University of Science and Technology, Al. Mickiewicza 30, 30-059 Kraków, Poland. [3]Faculty of Physics and Applied Computer Science, AGH University of Science and Technology, al. Mickiewicza 30, 30-059 Kraków, Poland. [4]Faculty of Physics, Adam Mickiewicz University, ul. Uniwersytetu Poznańskiego 2, 61-614 Poznań, Poland. ✉email: karwacki@ifmpan.poznan.pl; grochot@agh.edu.pl

No.	Sample	ρ_0^{H} ($\mu\Omega$cm)	ρ_0^{F} ($\mu\Omega$cm)	$\lvert\theta_{\mathrm{SH}}\rvert$ (%)	θ_{AMR} (%)	λ_{H} (nm)	λ_{F} (nm)
W1	W(5)/$Co_{20}Fe_{60}B_{20}(t_F)$/Ta(1)	185	144	22.5 ± 0.4	0.19 ± 0.03	1.3[a]	5[c]
W2	W(t_H)/$Co_{20}Fe_{60}B_{20}$(5)/Ta(1)	166	144	21 ± 1	0.07 ± 0.08	1.3[a]	5[c]
W3	W(5)/Co(t_F)/Ta(1)	120	22	≈ 0	1.1 ± 0.3	1.3[a]	7[c]
W4	W(t_H)/Co(5)/Ta(1)	120	30	23 ± 2	0.69 ± 0.02	1.3[a]	7[c]
P1	$Co_{20}Fe_{60}B_{20}(t_F)$/Pt(3)	95	102	16.0 ± 0.2	0.38 ± 0.01	2.2[a]	5[c]
P2	$Co_{20}Fe_{60}B_{20}$(5)/Pt(t_H)	151	161	6 ± 2	0.36 ± 0.03	2.2[a]	5[c]
P3	Co(t_F)/Pt(4)	55	18	≈ 0	0.5 ± 0.1	2.2[a]	7[b]
P4	Co(5)/Pt(t_H)	24	57	9 ± 1	1.5 ± 0.1	2.2[a]	7[b]
A1	Ti(2)/Au(5)/$Co_{20}Fe_{60}B_{20}(t_F)$/Ti(1.5)	24	96	3.3 ± 0.1	0.210 ± 0.008	1.6[a]	5[c]
A2	Ti(2)/Au(t_H)/CoFeB(5)/Ti(1.5)	15	96	5 ± 1	0.33 ± 0.05	1.6[a]	5[c]

Table 1. Composition of samples, and resistivities of heavy metal and ferromagnetic layers. Numbers in parentheses next to material symbol denote thickness (in nm) of the corresponding layer; parameters used for fitting the model to experimental data. [a]Ref. 38, [b]Ref. 39, [c]Ref. 40.

strength of the spin Hall effect) and spin diffusion length in different experimental schemes, for instance in spin-orbit torque ferromagnetic resonance (SOT-FMR)[37,38], relies heavily on the magnetoresistive properties of a system, it is important to properly determine all the contributions to magnetoresistance.

Here, we revisit the theory of spin Hall magnetoresistance in metallic bilayers by explicitly including the contribution from AMR into the spin drift-diffusion theory for the ferromagnetic metal layer. The expressions for magnetoresistance are then fitted to the data obtained from resistance measurements on heavy-metal (H)/ferromagnet (F) bilayers, where H: W, Pt, Au, while F: Co, $Co_{20}Fe_{60}B_{20}$. This allows us to determine more accurately contributions from various magnetotransport phenomena occurring in metallic bilayers where the spin Hall effect is the driving source. Such analysis may also be useful in the efforts to optimize prospective devices for information technology.

Results

This section is divided into two sections depending on the ferromagnetic material used in the bilayer. As $Co_{20}Fe_{60}B_{20}$ is amorphous and Co is crystalline, they present differently in magnetoresistance experiments and can influence the estimation of spin transport properties, especially when the thickness of ferromagnetic material is varied while thickness of heavy metal remains constant.

The spin Hall angles obtained from fitting for W, Pt, and Au, shown in Table 1, agree quite well with spin Hall angles for thick heavy metals obtained in spin-orbit torque ferromagnetic resonance experiments used in our previous papers[38,41]. Larger spin Hall angle for Pt-based bilayer P1, where the thickness of ferromagnetic metal varies, can be attributed to, f.i., changes in spin-mixing conductivity[17], which, as described above, we do not take into account in current approach.

$Co_{20}Fe_{60}B_{20}$-based bilayers. Figure 1 shows relative magnetoresistance as a function of heavy metal (Fig. 1a–c) and ferromagnetic metal (Fig. 1d–f) layer thicknesses for H/$Co_{20}Fe_{60}B_{20}$ bilayers where H: W, Pt, Au.

Dependence of magnetoresistance on heavy-metal thickness, with fixed $t_{\mathrm{F}} = 5$ nm, shown in Fig. 1a–c indicates, as expected, that SMR is the largest contribution to magnetoresistance in heterostructure with W as a heavy metal layer due to larger spin Hall angle of W, $\lvert\theta_{\mathrm{SH}}\rvert \approx 21\%$, compared to Pt, $\lvert\theta_{\mathrm{SH}}\rvert \approx 6\%$, and to Au, $\lvert\theta_{\mathrm{SH}}\rvert \approx 4\%$. Consequently, in Pt and Au bilayers AMR dominates over SMR.

The dependence of magnetoresistance on ferromagnetic layer thickness is shown in Fig. 1d–f. For 5 nm–thick W as heavy metal layer, shown in Fig. 1d SMR is still the dominating contribution to the total magnetoresistance in the studied thickness range. For device with 3 nm–thick Pt, the SMR for $t_{\mathrm{F}} \gtrsim 2$ nm is smaller than AMR. Note that for both W- and Pt-based bilayers the model fit and theoretical prediction do not describe the behavior of MR for $t_{\mathrm{F}} \lesssim 2$ nm, which can be attributed to strong dependence of the interfacial parameters such as spin-mixing conductance on thickness. Due to small spin Hall angle, SMR in Au-based is rather small and MR is dominated by AMR.

Co-based bilayers. Magnetoresistance and relative magnetoresistance in H/Co bilayers (H: W, Pt) are shown in Fig. 2 as a function of heavy metal (Fig. 2a,b) and ferromagnetic metal (Fig. 2c,d) layer thicknesses.

For W and Pt bilayers with varying heavy metal thickness and $t_{\mathrm{F}} = 5$ nm, shown in Fig. 2, the total magnetoresistance is mostly due to AMR, in contrast to $Co_{20}Fe_{60}B_{20}$–based bilayers described in the previous subsection.

For bilayers with varying ferromagnetic metal (Co) thickness, shown in Fig. 2c,d, the total magnetoresistance is also largely dominated by AMR.

Due to existence of a magnetic dead layer, disoriented crystalline structure of Co, and due to the fact that magnetization of Co does not lie completely in-plane of the sample for small thicknesses we introduced the magnetically effective thickness, $t_{\mathrm{F,eff}}$, of Co layer. More details on some of these aspects can be found in Supplementary Information. Since the thickness of heavy-metal is fixed and the thickness of the ferromagnetic metal

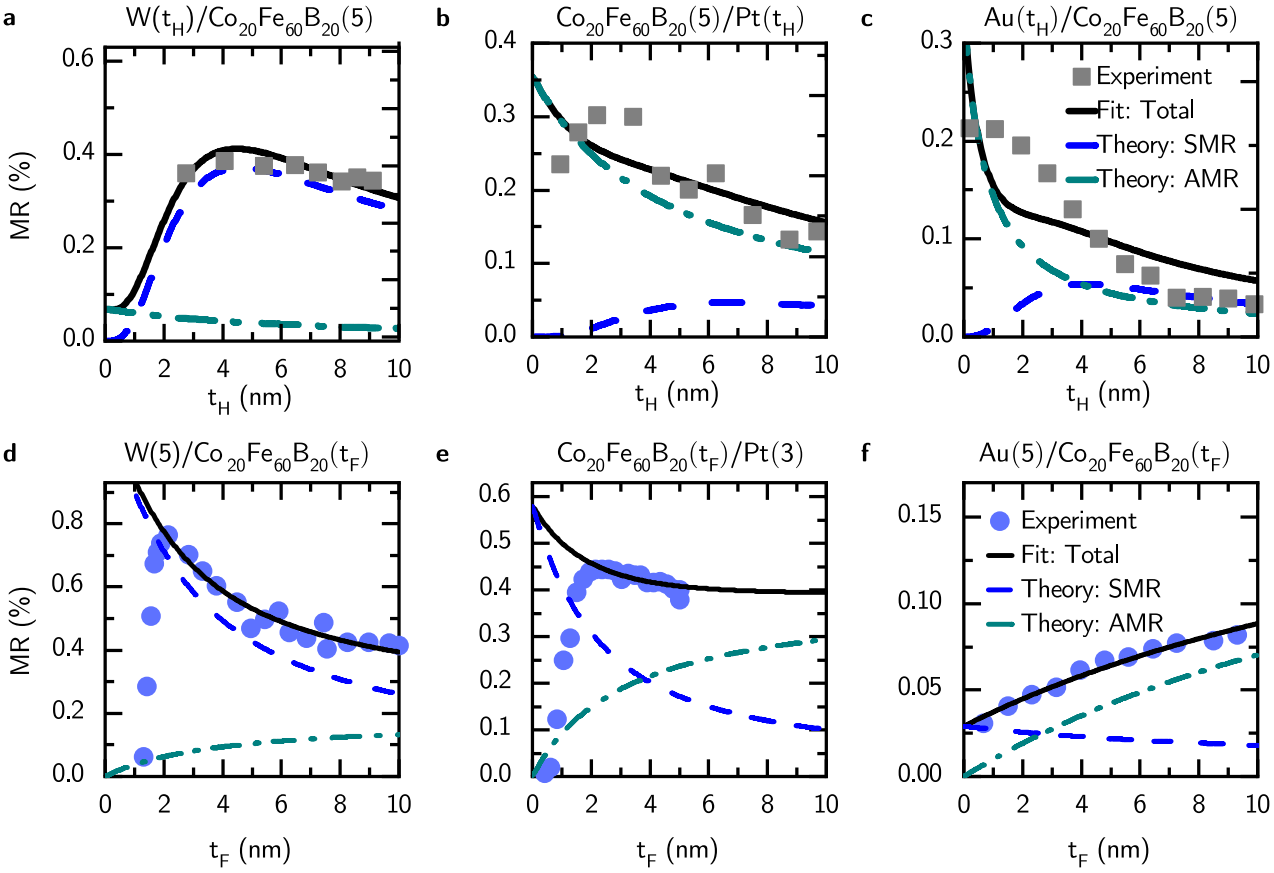

Fig. 1. Relative magnetoresistance, *MR*, as a function of heavy metal's thickness, t_H, for: **a**, $W/Co_{20}Fe_{60}B_{20}$, **b**, $Co_{20}Fe_{60}B_{20}/Pt$, and **c**, $Au/Co_{20}Fe_{60}B_{20}$ bilayers, and as a function of ferromagnetic metal's thickness, t_F, for: **d**, $W(5)/Co_{20}Fe_{60}B_{20}$, **e**, $Co_{20}Fe_{60}B_{20}/Pt(3)$, and **f**, $Au(5)/Co_{20}Fe_{60}B_{20}$ bilayers. Parameters used for theoretical curves are gathered in Table 1.

increases, the large differences in resistivities result in larger portion of charge current flowing into Co leading to negligible SMR—thus preventing proper estimation of spin Hall angle of both W and Pt.

Discussion

Our systematic analysis of magnetoresistance in in-plane magnetized heavy-metal/ferromagnetic-metal bilayers with crystalline Co and amorphous $Co_{20}Fe_{60}B_{20}$ has shown that proper choice of ferromagnetic-metal is crucial to the optimization of spin Hall magnetoresistance.

As shown in previous section, although W has larger spin Hall angle than Pt and Au, the magnetoresistance of $W/Co_{20}Fe_{60}B_{20}$ and even W/Co (for thin W) bilayers can be lower than that of Co/Pt bilayer due to high AMR contribution in the latter. This also leads to possible underestimation of SMR contribution which is lower in W/Co than in $W/Co_{20}Fe_{60}B_{20}$ bilayers, one of the main reasons for which is quite large difference in resistivities of both layers (see Table 1), due to the fact that here β-W phase is disoriented (amorphous-like) resulting in more current flowing through Co than W and on average smaller spin Hall effect (see Supplementary Information). Moreover, due to the fact that here W is mostly amorphous and Co crystalline, a different interface properties between these materials than between crystalline-crystalline or amorphous-amorphous bilayers can influence spin transport as well.

For materials with stronger spin-orbit coupling (W and Pt) and comparable resistivities to $Co_{20}Fe_{60}B_{20}$, one obtains higher magnetoresistance response with thinner ferromagnet. In the case of Au-based bilayer, whose resistivity is smaller than that of $Co_{20}Fe_{60}B_{20}$, one obtains higher magnetoresistance with thicker ferromagnet. The predicted SMR contribution for $Au/Co_{20}Fe_{60}B_{20}$ can be higher than the SMR contribution for $Co_{20}Fe_{60}B_{20}$ /Pt due to the fact that larger current density flows through Au than through Pt, thus increasing the spin Hall response.

The estimation of SMR in the case of metallic bilayers is hindered by large differences in resistivity of the constituent metallic layers. Since in this case AMR is strongly dominating, the total MR increases with increasing effective thickness of Co.

In conclusion, we have developed an extended model of magnetoresistance for magnetic metallic bilayers with in-plane magnetized ferromagnets, which explicitly includes SMR and AMR contributions. The model was then fitted to experimental data on magnetoresistance in: $W/Co_{20}Fe_{60}B_{20}$, $Co_{20}Fe_{60}B_{20}/Pt$, $Au/Co_{20}Fe_{60}B_{20}$, W/Co,

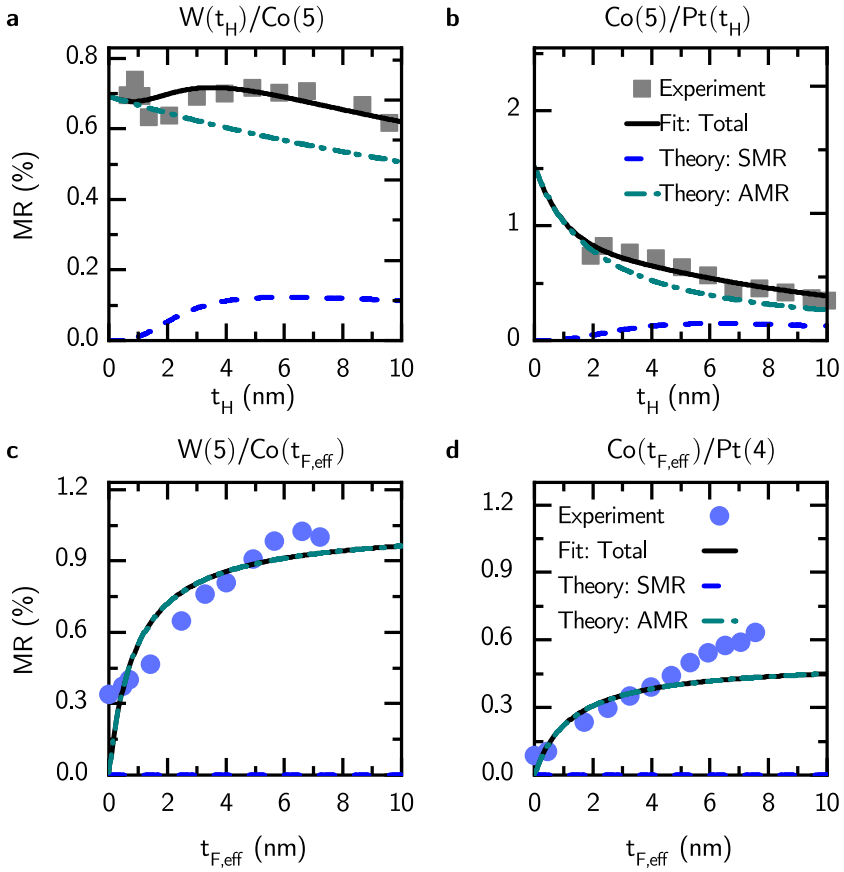

Fig. 2. Relative magnetoresistance, *MR*, as a function of heavy metal's thickness, t_H, for: **a**, W(t_H)/Co(5), **b**, Co(5)/Pt(t_H) bilayers, and as a function of ferromagnetic metal's effective thickness, $t_{F,eff}$, for: **c**, W(5)/Co($t_{F,eff}$), **d**, Co($t_{F,eff}$)/Pt(4) bilayers. Parameters used for theoretical curves are gathered in Table 1.

Co/Pt heterostructures, to estimate the strength of SMR and AMR effects. In particular, we have compared the influence of amorphous ferromagnet ($Co_{20}Fe_{60}B_{20}$) and crystalline ferromagnet (Co) on total magnetoresistance and analyzed the dependence of magnetoresistance on ferromagnet's thickness, which allows for better optimization of magnetic bilayers.

These results allow for a more accurate estimation of different contributions to magnetoresistance in magnetic metallic systems, which is important for applications in, e. g., spintronic SOT-devices[42] or in other experimental schemes that rely on magnetoresistance measurements in evaluation of the spin transport properties.

Methods

Experiment. Table 1 shows the multilayer systems that were produced for SMR studies. The magnetron sputtering technique was used to deposit multilayers on the Si/SiO_2 thermally oxidized substrates. Thickness of wedged layers were precisely calibrated by X-ray reflectivity (XRR) measurements. The details of sputtering deposition parameters as well as structural phase analysis of highly resistive W and Pt layers can be found in our recent papers[38,41]. Au in Au/$Co_{20}Fe_{60}B_{20}$ bilayers is (111) fcc textured similarly as Pt in $Co_{20}Fe_{60}B_{20}$/Pt bilayer[38]. In turn, structure analysis of the hcp-Co crystal phases grown on disoriented β-W can be found in the Supplementary Information.

After deposition, multilayered systems were nanostructured using either electron-beam lithography or optical lithography, ion etching and lift-off. The result was a matrix of Hall bars and strip nanodevices for further electrical measurements. The sizes of produced structures were: 100 μm x 10 μm or 100 μm x 20 μm. In order to ensure good electrical contact with the Hall bars and strips, Al(20)/Au(30) contact pads with dimensions of 100 μm x 100 μm were deposited. Appropriate placement of the pads allows rotation of the investigated sample and its examination at any angle with respect to the external magnetic field in a dedicated rotating probe station using a four-points probe. The constant magnetic field, controlled by a gaussmeter exceeded magnetization saturation in plane of the sample and the sample was rotated in an azimuthal plane from $-120°$ to $+100°$.

The resistance of the system was measured with a two- and four-point technique using Keithley 2400 sourcemeters and Agilent 34401A multimeter. As shown in Supplementary Information, resistances of bilayers with amorphous ferromagnet $Co_{20}Fe_{60}B_{20}$ are about one order higher than these with polycrystalline Co. The same results were obtained using both methods. The thickness-dependent resistivity of individual layers was determined by method described in Ref. 7, and by a parallel resistors model. For more details on resistivity measurements we refer the reader to Supplementary Information.

Theory. To properly assess all contributions to magnetoresistance one should find first the average current density flowing through the whole heterostructure. This approach, in contrast to the one described in Ref. 5 allows one to properly describe magnetoresistance in more complicated heterostructures, where *ad hoc* addition of consitutent terms might lead to oversimplification and improper determination of different components in the magnetoresistance. Moreover, calculating average current density allows for a phenomenological description of how various magnetoresistance effects depend on thicknesses of the constituent layers. The drawback, however, is the necessary simplification of fitting parameters, which we discuss in more detail in the next subsection devoted to fitting procedure.

Only the component flowing along the normal to interfaces is relevant and will be taken into account in the following, i.e.

$$\mathbf{j}_s^{\mathrm{H}}(z) = -\frac{\theta_{\mathrm{SH}}}{\rho_0^{\mathrm{H}}}\hat{\mathbf{e}}_z \times \mathbf{E} + \frac{1}{2e\rho_0^{\mathrm{H}}}\frac{\partial \boldsymbol{\mu}_s^{\mathrm{H}}(z)}{\partial z}\,. \tag{1}$$

Here θ_{SH} is the spin Hall angle, ρ_0^{H} is the bare resistivity of the heavy metal, and $\boldsymbol{\mu}_s^{\mathrm{H}}(z)$ is the spin accumulation that is generally z-dependent.

The charge current density in the heavy-metal (H) layer, in turn, can be written in the form

$$\mathbf{j}_c^{\mathrm{H}}(z) = \frac{1}{\rho_0^{\mathrm{H}}}\mathbf{E} + \frac{\theta_{\mathrm{SH}}}{2e\rho_0^{\mathrm{H}}}\hat{\mathbf{e}}_z \times \frac{\partial \boldsymbol{\mu}_s^{\mathrm{H}}(z)}{\partial z}\,, \tag{2}$$

and contains the bare charge current density and the current due to inverse spin Hall effect. Note, that the spin current in general can induce charge current also flowing along the axes x and y. However, due to lateral dimensions of the samples much larger than the layer thicknesses and spin diffusion lengths, those additional components can be neglected.

Thus, one can write[28,29]:

$$\mathbf{j}_s^{F}(z) = \frac{1}{2e\rho_0^{\mathrm{F}}}\nabla\mu_s^{\mathrm{F}}(z) + \frac{\beta}{2e\rho_0^{\mathrm{F}}}\nabla\mu_c^{\mathrm{F}}(\mathbf{r}) - \frac{\theta_{\mathrm{AMR}}}{2e\rho_0^{\mathrm{F}}}\hat{\mathbf{m}}\left[\hat{\mathbf{m}}\cdot\nabla\mu_s^{\mathrm{F}}(z)\right], \tag{3}$$

in which θ_{AMR} is the AMR angle, defined as $\theta_{\mathrm{AMR}} = \sigma_{\mathrm{AMR}}\rho_0^{\mathrm{F}}$, while $\mu_c^{\mathrm{F}}(\mathbf{r}) = 2e\mathbf{E}\cdot\mathbf{r} + \mu_c^{F}(z)$ is the electrochemical potential.

Charge current density in the ferromagnetic layer (F) can be written as[28,29],

$$\mathbf{j}_c^{F}(z) = \frac{1}{2e\rho_0^{\mathrm{F}}}\nabla\mu_c^{\mathrm{F}}(\mathbf{r}) + \frac{\beta}{2e\rho_0^{\mathrm{F}}}\nabla\mu_s^{\mathrm{F}}(z) - \frac{\theta_{\mathrm{AMR}}}{2e\rho_0^{\mathrm{F}}}\hat{\mathbf{m}}\left[\hat{\mathbf{m}}\cdot\nabla\mu_c^{\mathrm{F}}(\mathbf{r})\right]. \tag{4}$$

Note, in the above equations the current densities in both H and F layers we assumed as linear response to electric field, i.e. we neglected the so-called unidirectional spin Hall magnetoresistance effect[24–27].

The spin current $\mathbf{j}_s^{\mathrm{HF}}$ flowing through the heavy-metal/ferromagnet interface is given by the following expression [43]:

$$\mathbf{j}_s^{\mathrm{HF}} = G_F\left[\left(\boldsymbol{\mu}_s^{\mathrm{F}}(0) - \boldsymbol{\mu}_s^{\mathrm{H}}(0)\right)\cdot\hat{\mathbf{m}}\right]\hat{\mathbf{m}} + G_r\hat{\mathbf{m}}\times\hat{\mathbf{m}}\times\boldsymbol{\mu}_s^{\mathrm{H}}(0)\,. \tag{5}$$

Here $G_F = (1-\gamma^2)(G_\uparrow + G_\downarrow)/2$ with γ defined as $\gamma = (G_\uparrow - G_\downarrow)/(G_\uparrow + G_\downarrow)$ and $G_\uparrow$ and $G_\downarrow$ denoting the interface conductance for spin-↑ and spin-↓. Furthermore, $G_r \equiv \mathrm{Re}G_{\mathrm{mix}}$ and $G_i \equiv \mathrm{Im}G_{\mathrm{mix}}$, where G_{mix} is the so-called spin-mixing conductance. Note, that we neglect explicitly a contribution from the interfacial Rashba-Edelstein spin polarization[38]. A strong interfacial spin-orbit contribution which induces spin-flip processes can also be combined with the interfacial spin conductance G_F as a spin-conductance reducing parameter $1-\eta$, with $\eta = 0$ for no interfacial spin-orbit coupling, and $\eta = 1$ for maximal spin-orbit coupling. Note, that this reduction could also be attributed to the magnetic proximity effect, especially in the case of Pt-based heterostructures[13], however recent studies suggest its irrelevance for spin-orbit-torque–related experiments[22]. In the following discussion we assume $\eta = 0$ and treat G_F as an effective parameter.

To find charge and spin currents we need to find first the spin accumulation at the H/F interface and also at external surface/interfaces. This can be found from the following boundary conditions:

$$\mathbf{j}_s^{\mathrm{H}}(z = -t_H) = 0\,, \tag{6a}$$

$$\mathbf{j}_s^{\mathrm{F}}(z = t_F) = 0\,, \tag{6b}$$

$$\mathbf{j}_s^{\mathrm{H}}(z = 0) = \mathbf{j}_s^{\mathrm{HF}}\,, \tag{6c}$$

$$j_{s,z}^{\mathrm{F}}(z = 0) = \mathbf{j}_s^{\mathrm{HF}}\cdot\hat{\mathbf{m}}\,. \tag{6d}$$

Having found electrochemical potential and spin accumulation from general solution

$$\mu_s^{F,H}(z) = \mathbf{A}_{F,H}e^{-z/\lambda_{F,H}} + \mathbf{B}_{F,H}e^{z/\lambda_{F,H}}\,, \tag{7}$$

where $\mathbf{A}_{F,H}$ and $\mathbf{B}_{F,H}$ are coefficients to be determined and $\lambda_{F,H}$ is the spin diffusion length in ferromagnet or heavy metal, one can find the longitudinal in-plane components of the averaged charge current $\mathbf{j}(\hat{\mathbf{m}})$ from the formula:

$$j_{xx}(\hat{\mathbf{m}}) = \frac{1}{t_H + t_F}\left[\int_{t_H} dz\hat{\mathbf{e}}_x \cdot \mathbf{j}_c^{\mathrm{H}}(z) + \int_{t_F} dz\hat{\mathbf{e}}_x \cdot \mathbf{j}_c^{\mathrm{F}}(z)\right]. \tag{8}$$

The total longitudinal charge current can be written down in the Ohm's-law form,

$$j_{xx}(\hat{\mathbf{m}}) = \frac{1}{\rho_{xx}(\hat{\mathbf{m}})}E_x\,, \tag{9}$$

where the longitudinal resistivity is defined as follows:

$$\frac{1}{\rho_{xx}(\hat{\mathbf{m}})} = \sigma_0 + \sigma_x m_x^2 + \sigma_y m_y^2 \tag{10}$$

with

$$\sigma_0 \approx \frac{\rho_0^{\mathrm{F}} t_H + \rho_0^{\mathrm{H}} t_F}{\rho_0^{\mathrm{F}}\rho_0^{\mathrm{H}} t_F + \rho_0^{\mathrm{F}}\rho_0^{\mathrm{H}} t_H} \tag{11}$$

$$\begin{aligned}\sigma_x &= \frac{\theta_{\mathrm{SH}}^2}{\rho_0^{\mathrm{H}}}\frac{g_{\mathrm{DL}}\lambda_{\mathrm{H}}}{t_F + t_H}\tanh\left(\frac{t_H}{2\lambda_{\mathrm{H}}}\right) - \frac{\theta_{\mathrm{AMR}}}{\rho_0^{\mathrm{F}}}\frac{t_F}{t_F + t_H}\,,\\ &= \sigma_x^{\mathrm{SH}} + \sigma_x^{\mathrm{AMR}}\,,\end{aligned} \tag{12}$$

$$\sigma_y = \frac{\theta_{\mathrm{SH}}^2}{\rho_0^{\mathrm{H}}}\frac{g_H^{\mathrm{F}}\lambda_{\mathrm{H}}}{t_F + t_H}\tanh\left(\frac{t_H}{2\lambda_{\mathrm{H}}}\right). \tag{13}$$

In the above expressions the following dimensionless coefficients have been introduced to simplify the notation:

$$g_{\mathrm{DL}} = \left[1 - \mathrm{sech}\left(\frac{t_H}{\lambda_{\mathrm{H}}}\right)\right]\frac{g_r(1+g_r) + g_i^2}{(1+g_r)^2 + g_i^2}\,, \tag{14}$$

$$g_{r,i} = 2G_{r,i}\rho_0^{\mathrm{H}}\lambda_{\mathrm{H}}\coth\left(\frac{t_H}{\lambda_{\mathrm{H}}}\right), \tag{15}$$

$$g_H^{\mathrm{F}} = \left[1 - \mathrm{sech}\left(\frac{t_H}{\lambda_{\mathrm{H}}}\right)\right]\frac{1}{1 + \left(\frac{1}{2G_F\lambda_{\mathrm{H}}\rho_0^{\mathrm{H}}} + \gamma_H^{\mathrm{F}}\right)\tanh\left(\frac{t_H}{\lambda_{\mathrm{H}}}\right)}\,, \tag{16}$$

$$\gamma_H^{\mathrm{F}} = \frac{\lambda_{\mathrm{F}}\rho_0^{\mathrm{F}}}{\lambda_{\mathrm{H}}\rho_0^{\mathrm{H}}(1-\beta^2)}\coth\left(\frac{t_F}{\lambda_{\mathrm{F}}}\right). \tag{17}$$

With the resistivity defined in Eq. (10) we can now define magnetoresistance,

$$MR = \frac{\rho_{xx}(\hat{\mathbf{m}} \parallel \hat{\mathbf{e}}_x) - \rho_{xx}(\hat{\mathbf{m}} \parallel \hat{\mathbf{e}}_y)}{\rho_{xx}(\hat{\mathbf{m}} \parallel \hat{\mathbf{e}}_x)}\,, \tag{18}$$

Taking into account Eqs. (11)-(13), the above formula can be written as,

$$MR \approx \frac{\sigma_y - \sigma_x}{\sigma_0}\,. \tag{19}$$

In order to compare the models with and without AMR, we define SMR as:

$$SMR = MR\Big|_{\theta_{\mathrm{AMR}}\to 0} = \frac{\sigma_y^{\mathrm{SH}} - \sigma_x^{\mathrm{SH}}}{\sigma_0}\,, \tag{20}$$

which simplifies our model to that introduced by Kim et al. 5. We also define AMR coefficient

$$AMR = MR\Big|_{\theta_{\mathrm{SH}}\to 0} = -\frac{\sigma_x^{\mathrm{AMR}}}{\sigma_0}\,. \tag{21}$$

Fitting procedure. In order to analyze the experimental data in light of our extended model, we fit Eq. (19) to the data on relative magnetoresistance. We have assumed some constant values according to literature and

our previous works: spin polarization at Fermi level of both Co and $Co_{20}Fe_{60}B_{20}$ are taken as $\beta = 0.3$. Note that this value can range in $Co_{20}Fe_{60}B_{20}$ from 0.1 to 0.6[40] and can influence the fit of the model to the data. We have assumed spin diffusion lengths in Pt and W from our previous papers[38,41] to be 2.2 nm and 1.3 nm, respectively. For $Co_{20}Fe_{60}B_{20}$ we assumed constant room-temperature value of $\lambda_F \approx 5$ nm [40] and for Co $\lambda_F \approx 7$ nm[39]. Note, that we have assumed constant effective spin diffusion lengths for the constituent layers obtained from our previous analyses [38,41]. In general, however, these parameters can depend on temperature or thickness of the layers[44,45]. This fact can lead to underestimation of spin diffusion lengths and overestimation of the spin Hall angles. One of the remedies might be to use effective thickness-dependent parameters[45]. However, such approaches are still mostly empirical and not based on proper theoretical grounding and as such have their own limitations.

Moreover we have assumed transparent contacts for spin transport, i.e. $G_F \to \infty$ and $G_r \to \infty$, and also assumed G_i to be negligible. These assumptions are mostly valid for metallic interfaces. However, these parameters can also strongly depend on type of interface, i.e. they can differ in amorphous/crystalline (f.i. $Co_{20}Fe_{60}B_{20}$/Pt), crystalline/crystalline (Co/Pt), and amorphous-like/amorphous (f.i. W/$Co_{20}Fe_{60}B_{20}$) heterostructures.

We have assumed spin Hall angle θ_{SH} and AMR coefficient θ_{AMR} as fitting parameters and the results of fitting the model to the experimental data on magnetoresistance are gathered in Table 1. Morevoer, we have assumed anomalous Hall effect to be negligible in the in-plane magnetized systems considered in the paper. This effect might play an important role for ferromagnets with stronger spin-orbit coupling or ferromagnets tilted out of plane[28–30].

Received: 7 February 2020; Accepted: 8 June 2020
Published online: 01 July 2020

References

1. Althammer, M. et al. Quantitative study of the spin Hall magnetoresistance in ferromagnetic insulator/normal metal hybrids. Phys. Rev. B 87, 224401 (2013).
2. Nakayama, H. et al. Spin Hall magnetoresistance induced by a nonequilibrium proximity effect. Phys. Rev. Lett. 110, 206601 (2013).
3. Chen, Y.-T. et al. Theory of spin Hall magnetoresistance. Phys. Rev. B 87, 144411 (2013).
4. Chen, Y.-T. *et al.* Theory of spin Hall magnetoresistance (SMR) and related phenomena. *J. Phys. Condens. Matt.***28**, 103004 (2016).
5. Kim, J., Sheng, P., Takahashi, S., Mitani, S. & Hayashi, M. Spin Hall magnetoresistance in metallic bilayers. Phys. Rev. Lett. 116, 097201 (2016).
6. Choi, J.-G., Lee, J. W. & Park, B.-G. Spin Hall magnetoresistance in heavy-metal/metallic-ferromagnet multilayer structures. Phys. Rev. B 96, 174412 (2017).
7. Kawaguchi, M., Towa, D., Lau, Y. C., Takahashi, S. & Hayashi, M. Anomalous spin Hall magnetoresistance in Pt/Co bilayers. Appl. Phys. Lett. 112, 202405 (2018).
8. Avci, C. O., Beach, G. S. D. & Gambardella, P. Effects of transition metal spacers on spin-orbit torques, spin hall magnetoresistance, and magnetic anisotropy of pt/co bilayers. *Phys. Rev. B***100**, (2019).
9. Lv, Y. et al. Unidirectional spin-Hall and Rashba-Edelstein magnetoresistance in topological insulator-ferromagnet layer heterostructures. Nat. Commun. 9, 111 (2018).
10. Narayanapillai, K. et al. Interfacial Rashba magnetoresistance of the two-dimensional electron gas at the LaAlO3 / SrTiO3 interface. Phys. Rev. B 96, 064401 (2017).
11. Hirsch, J. E. Spin Hall effect. Phys. Rev. Lett. 83, 1834–1837 (1999).
12. Dyakonov, M. I. Magnetoresistance due to edge spin accumulation. Phys. Rev. Lett. 99, 126601 (2007).
13. Huang, S. Y. et al. Transport magnetic proximity effects in platinum. Phys. Rev. Lett. 109, 107204 (2012).
14. Sinova, J., Valenzuela, S. O., Wunderlich, J., Back, C. H. & Jungwirth, T. Spin Hall effects. Rev. Mod. Phys. 87, 1213 (2015).
15. Liu, Y., Zhou, B. & Zhu, J.-G. Field-free magnetization switching by utilizing the spin Hall effect and interlayer exchange coupling of iridium. Sci. Rep. 9, 325 (2019).
16. Kobs, A. et al. Anisotropic interface magnetoresistance in Pt/Co/Pt sandwiches. Phys. Rev. Lett. 106, 217207 (2011).
17. Pai, C.-F., Ou, Y., Vilela-Leão, L. H., Ralph, D. C. & Buhrman, R. A. Dependence of the efficiency of spin Hall torque on the transparency of Pt/ferromagnetic layer interfaces. Phys. Rev. B 92, 064426 (2015).
18. Zhang, W., Han, W., Jiang, X., Yang, S.-H. & Parkin, S. S. P. Role of transparency of platinum–ferromagnet interfaces in determining the intrinsic magnitude of the spin Hall effect. Nat. Phys. 11, 496–502 (2015).
19. Zhang, S. S.-L., Vignale, G. & Zhang, S. Anisotropic magnetoresistance driven by surface spin-orbit scattering. Phys. Rev. B 92, 024412 (2015).
20. Tokaç, M. et al. Interfacial contribution to thickness dependent in-plane anisotropic magnetoresistance. AIP Advances 5, 127108 (2015).
21. Tokaç, M. et al. Interfacial structure dependent spin mixing conductance in cobalt thin films. Phys. Rev. Lett. 115, 056601 (2015).
22. Zhu, L. J., Ralph, D. C. & Buhrman, R. A. Irrelevance of magnetic proximity effect to spin-orbit torques in heavy-metal/ferromagnet bilayers. Phys. Rev. B 98, 134406 (2018).
23. Amin, V. P., Zemen, J. & Stiles, M. D. Interface-generated spin currents. Phys. Rev. Lett. 121, 136805 (2018).
24. Avci, C. O. et al. Unidirectional spin Hall magnetoresistance in ferromagnet/normal metal bilayers. Nat. Phys. 11, 570–575 (2015).
25. Avci, C. O. et al. Magnetoresistance of heavy and light metal/ferromagnet bilayers. Appl. Phys. Lett. 107, 192405 (2015).
26. Zhang, S. S.-L. & Vignale, G. Theory of unidirectional spin Hall magnetoresistance in heavy-metal/ferromagnetic-metal bilayers. Phys. Rev. B 94, 140411(R) (2016).
27. Avci, C. O., Mendil, J., Beach, G. S. D. & Gambardella, P. Origins of the unidirectional spin Hall magnetoresistance in metallic bilayers. Phys. Rev. Lett. 121, 087207 (2018).
28. Taniguchi, T., Grollier, J. & Stiles, M. D. Spin-transfer torques generated by the anomalous Hall effect and anisotropic magnetoresistance. Phys. Rev. Appl. 3, 044001 (2015).
29. Taniguchi, T. Magnetoresistance generated from charge-spin conversion by anomalous Hall effect in metallic ferromagnetic/nonmagnetic bilayers. Phys. Rev. B 94, 174440 (2016).
30. Yang, Y. et al. Anomalous Hall magnetoresistance in a ferromagnet. Nat. Commun. 9, 2255 (2018).
31. Jan, J.-P. Galvamomagnetic and thermomagnetic effects in metals. In *Solid State Physics*, 1–96 (Elsevier, 1957).
32. McGuire, T. & Potter, R. Anisotropic magnetoresistance in ferromagnetic 3d alloys. IEEE Trans. Magn. 11, 1018–1038 (1975).
33. Bass, J. & Pratt, W. P. Spin-diffusion lengths in metals and alloys, and spin-flipping at metal/metal interfaces: an experimentalist's critical review. *J. Phys. Condens. Mat.***19**, 183201 (2007).

34. Bechthold, P. S. Galvanomagnetic transport: from Hall effect to AMR. In Blügel, S., Bürgler, D., Morgenstern, M., Schneider, C. M. & Waser, R. (eds.) Spintronics - From GMR to Quantum Information. Institute of Solid State Research, Forschungszentrum Jülich (Forschungszentrum Jülich GmbH, Jülich, 2009).
35. Nagaosa, N., Sinova, J., Onoda, S., MacDonald, A. H. & Ong, N. P. Anomalous Hall effect. Rev. Mod. Phys. 82, 1539 (2010).
36. Iihama, S. et al. Spin-transfer torque induced by the spin anomalous Hall effect. Nat. Electron. 1, 120–123 (2018).
37. Liu, L., Moriyama, T., Ralph, D. C., & Buhrman, R. A. Spin-torque ferromagnetic resonance induced by the spin Hall effect. Phys. Rev. Lett. 106, 036601 (2011).
38. Skowroński, W. et al. Determination of spin Hall angle in heavy-metal/Co-Fe-B-based heterostructures with interfacial spin-orbit fields. Phys. Rev. Appl. 11, 024039 (2019).
39. Zahnd, G. et al. Spin diffusion length and polarization of ferromagnetic metals measured by the spin-absorption technique in lateral spin valves. Phys. Rev. B 98, 174414 (2018).
40. Ahn, C., Shin, K. H. & Pratt, W. P. Magnetotransport properties of CoFeB and Co/Ru interfaces in the current-perpendicular-to-plane geometry. Appl. Phys. Lett. 92, 102509 (2008).
41. Łazarski, S. et al. Field-free spin-orbit-torque switching in Co/Pt/Co multilayer with mixed magnetic anisotropies. Phys. Rev. Appl. 12, 014006 (2019).
42. Manchon, A. *et al.* Current-induced spin-orbit torques in ferromagnetic and antiferromagnetic systems. *Rev. Mod. Phys.***91**, (2019).
43. Brataas, A., Bauer, G. & Kelly, P. Non-collinear magnetoelectronics. Phys. Rep. 427, 157–255 (2006).
44. Cecot, M. et al. Influence of intermixing at the Ta/CoFeB interface on spin hall angle in Ta/CoFeB/MgO heterostructures. Sci. Rep. 7, 968 (2017).
45. Swindells, C., Hindmarch, A. T., Gallant, A. J. & Atkinson, D. Spin transport across the interface in ferromagnetic/nonmagnetic systems. Phys. Rev. B 99, 064406 (2019).

Acknowledgements

This work is supported by the National Science Centre in Poland Grant UMO-2016/23/B/ST3/01430 (SPINORBITRONICS). WS acknowledges National Science Centre in Poland Grant No. 2015/17/D/ST3/00500. JK and WP acknowledge National Science Centre in Poland Grant No. 2012/05/E/ST7/00240. The nanofabrication process was performed at the Academic Centre for Materials and Nanotechnology (ACMiN) of AGH University of Science and Technology. The authors thank M. Schmidt for technical support.

Author contributions

KG, SŁ, and WS fabricated Hall-bars in the clean-room and carried out electrical measurements, FS provided the samples, JK and WP, performed and analyzed XRD and XRR data. ŁK and JB developed the theory, ŁK, TS and JB, analyzed the results. All authors reviewed the manuscript.

Competing interests

The authors declare no competing interests.

Additional information

Supplementary information is available for this paper at https://doi.org/10.1038/s41598-020-67450-3.

Correspondence and requests for materials should be addressed to Ł.K. or K.G.

Reprints and permissions information is available at www.nature.com/reprints.

Publisher's note Springer Nature remains neutral with regard to jurisdictional claims in published maps and institutional affiliations.